# The rise of bubbles in shear thinning viscoelastic fluids

Q. Chen, Frederic Restagno, Dominique Langevin, A. Salonen

# The rise of bubbles in shear thinning viscoelastic fluids

Q. Chen [1], F. Restagno [1], D. Langevin [1], A. Salonen [1]

[1] Université Paris Saclay, CNRS, Laboratoire de Physique des Solides, France

E-mail: qizhou.chen@universite-paris-saclay.fr, anniina.salonen@universite-paris-saclay.fr

## ABSTRACT

*Hypothesis*

Bubbles in a liquid rise under gravity and separate to the top. Bubbly liquids exist commonly in nature and play a significant role in energy-conversion, oil and chemical industries. Therefore, understanding how bubbles rise is of great importance. Rheological properties of the fluid have a strong impact on single bubble rise and have been shown to change collective bubble rise at low gas volume fractions significantly. We expect that a viscoelastic fluid can strongly modify the rise of bubbles in more concentrated suspensions.

*Experiments*

We generate bubbly liquids up to gas fractions of 30 %. We measure the bubble size and the rise velocity in micellar solutions made of cetyltrimethylammonium bromide (CTAB) and sodium salicylate (NaSal), a common system to create shear-thinning solutions.

*Findings*

We show that when the NaSal concentration is small and the solutions are Newtonian, the bubble rise velocity decreases with increasing volume fraction of bubbles and the relationship between the two follows the Richardson-Zaki prediction. For the shear thinning viscoelastic solutions, the Richardson-Zaki relation no longer applies. Bubble clustering leads to faster rise velocities and a weaker dependence on the bubble volume fraction. At the largest concentration two rise regimes are observed. A fast one similar to that in the other shear thinning samples, followed by a very slow bubble rise. The slow rise velocity is attributed to the smallest bubbles rising so slowly that the shear rates around them lead to the fluid behaving as a Newtonian fluid. Therefore, bubble rise becomes again comparable to the Stokes expectations. We also show that the peculiar dependence of the rise velocity with volume fraction of bubbles in the shear thinning viscoelastic solutions can have important implications in flotation as the area flux changes strongly with bubble volume fraction.

**Keywords:** bubbly liquid, shear thinning viscoelastic fluids, bubble rise

## 1. Introduction

Gravity driven bubbly flows have received much attention during the past years. They have many practical applications, fizzy drinks, flotation for the recovery of minerals and water purification, reactors in the food, pharmaceutical and other industries. The role of the bubbles can be active to fix impurities or passive to change the fluid texture. Due to the large density difference between the liquid and the gas, in most cases bubbles will rise. In flotation, this allows to concentrate the material to be separated from the solution in the foam at the top. In many applications, the fluids are non-Newtonian which brings changes to the bubble dynamics in ways that are not fully understood yet [1]

The first investigations focused on single spherical bubbles rising in water [2]. It was observed that the rising velocity was the same as for solid particles of the same radius. Larger velocities were however expected for bubbles with mobile surfaces due to air recirculation in the interior. It was then postulated that there were surface active contaminants in water that created a viscous surface layer and immobilised the surface. Levich showed later that the surface immobilization was rather due to surface tension gradients created by the contaminants [3]. In thoroughly purified water and fluids with lower surface tension (that are less prone to contamination) the bubble surfaces are mobile. Further studies evidenced the important influence of the bubble size on the expression of the rising velocity. Millimetric bubbles indeed rise very fast and Stokes velocity is valid only at low Reynolds numbers. Large bubbles also deform in the flow, and flatten as they rise. Refined calculations describe well the rising motion of single bubbles in Newtonian fluids [4]. Note that small bubbles may shrink under the action of capillary pressure [5]. The rising motion in non-Newtonian fluids is less well understood [1]. Instead of flattening, bubbles may elongate in the flow and form large cusps. Their velocity increases sharply above a certain bubble size, a phenomenon not fully understood yet. It could be due in part to a change in boundary conditions at the bubble surface from immobile to mobile.

The motion of groups of bubbles is still more difficult to account for. A rising bubble creates flow in the surrounding fluid (or changes the velocities in its surroundings if the fluid is flowing), thus neighbouring bubbles are affected. When the bubbles are millimetric or larger, liquid circulation may occur, and the flow may become turbulent. Coalescence of bubbles is then important, but bubble break-up may occur due to turbulence and a dynamic equilibrium may establish [6]. When the fluid is viscoelastic, two bubbles are attracted, mostly due to normal stress differences that modify the pressure distribution at the bubbles surface. Bubble dimers rotate in order to minimize the hydrodynamic drag and bubble clusters form. When the

fluid is shear thinning, the fluid in the wake of a bubble has a smaller viscosity, and a bubble below can catch up, also leading to bubble attraction and formation of clusters. Elongation effects may lead to bubble separation when they are too close and a steady state separation can be observed. The formation of clusters leads to an increase of the rise velocity with bubble volume fraction $\phi$ as evidenced in measurements performed with small fractions, up to 1%. A maximum has been reported in a particular shear thinning fluid at $\phi \sim 0.5\%$, but no quantitative explanation of these findings have been proposed[1].

In the present paper, we extend the experiments to larger gas volume fractions, up to 30%. We use fluids made of wormlike micelles. These are surfactant micelles made with CTAB, (hexadecyl trimethyl ammonium bromide) that elongate upon addition of a salt, sodium salicylate (NaSal) which has a strong affinity for the micelle surface. When this salt is added, the viscosity of the solution increases but remains Newtonian if the salt concentration is small; at larger amounts of salt, the micelles entangle and the solutions become strongly viscous and shear thinning [7]. Recently Kostrezwa et al explored single particle sedimentation in CTAB/NaSal mixtures (4 mm stainless steel sphere), where they found an increase of the sedimentation velocity with decreasing micellar length in agreement with lower viscosities [8]. We chose these solutions in order to compare the behaviour of bubbles in Newtonian and non-Newtonian fluids. We used very small bubbles, in order to avoid bubble deformation. Their size is sufficiently small to remain in the regime of small Reynolds numbers. Coalescence is avoided due to the presence of surfactant. The surfactant also ensures that the bubble surfaces remain immobile. In this way, we simplify the hydrodynamic behaviour as much as possible and focus on the observation of the influence of the non-Newtonian behaviour of the suspending liquid.

## 2. Materials and Methods

### 2.1. Materials

The surfactant cetyltrimethylammonium bromide (CTAB) was purchased from Sigma-Aldrich with 99 % purity. Sodium salicylate (NaSal) was purchased from VWR with 100 % purity. They were used without further purification. Ultrapure water with a resistivity of 18.2 MΩ·cm produced using a Veolia water purification system was used to prepare all samples.

### 2.2.Sample preparation

Series of solutions were prepared with 20 mM of CTAB and increasing concentrations of NaSal (0-13 mM) by adding ultrapure water into the weighed compounds. The solutions were sonicated in a Branson 3510 Ultrasonic Cleaner for 1 h to homogenise the solution. The solutions were stored at room temperature (22 °C) for at least 24 h to ensure equilibration.

### 2.3.Rheology

The viscosity of the samples was measured using an MCR302 rheometer (Anton Paar, Graz, Austria). A cone plate system (CP50-2) with a radius of 50 mm and a taper angle of 2 ° was used. The temperature is controlled with a Peltier plate and set to 22 °C. The samples were inserted in the rheometer about 5 min before the measurement. Flow curves were measured at increasing shear rates from 0.01 $s^{-1}$ to 1000 $s^{-1}$. The shear moduli were measured with a constant strain of $\gamma = 1$ %.

### 2.4.Generation of bubbly liquids

Bubbly liquids were prepared using the double syringe method, which has been characterised by Gaillard et al [9]. Two 10 mL syringes from Fisher scientific were used with a tube connector with an inner radius of 2 mm. The CTAB/NaSal mixed solutions were poured into the syringe directly. The gas fraction of air was measured using the syringe indicators, and is known to ± 2 %. The syringe pistons were pushed back and forth 30 times for each sample to obtain bubbles of well-defined radius (typically between 15 and 40 µm). The gas fraction $\varphi_{gas}$ was varied between 5 % and 30 % in the samples.

### 2.5. Bubble size

A Malvern Mastersizer laser granulometer (Malvern Instruments, France) was employed to measure the surface weighted mean radius of the bubbles ($R_{32}$, Sauter radius). The sample

dispersion unit was filled with 10 mM CTAB solution, this concentration was sufficient to ensure that the bubbles were stable during measurement but less wasteful of CTAB as each measurement requires two litres of solution. After generation of the bubbles, the samples were transferred into the sample dispersion unit of Mastersizer with the stirring speed 1000 r/min. The bubble size was measured 10 times with a 3 s measurement time and an average taken.

### 2.6.Bubble rise velocity

After preparation, the bubbly liquids were immediately transferred into glass vials. A Ueye camera was used to observe the bubble rise. The time interval between images was 30 seconds for most experiments, but for samples with very fast bubble rise the interval was decreased to 5 seconds.

The Image J software was used to analyse the photographs, monitoring the grey scale *I* of pixels. In order to locate the front accurately, we determined the front position corresponding to different grey values. The details on how to obtain the average grey value of a certain area and the corresponding front position can be found in Figure S1 of the Supporting Information.

### 2.7.Surface tension

The surface tension experiments were performed with a Tracker instrument (Teclis, France) at 20 °C in the rising bubble configuration A bubble was created and the surface tension was measured during 10 minutes at which point it had reached its equilibrium value for all of the samples and no longer changed. These values are shown in Table 1.

Table 1. Surface tension of mixed CTAB/NaSal solutions. CTAB concentration: 20 mM

| NaSal concentration (mM) | 0 | 4 | 10 | 13 |
|---|---|---|---|---|
| Surface tension (mN/m) ± 0.5 mN/m | 35.1 | 31.5 | 27.4 | 27.0 |

The surface tension decreases when the NaSal concentration increases, a common effect for salts (They screen the electrostatic repulsion between surfactant polar heads, the surface layer becoming more compact.)

## 3. Results and Discussion

### 3.1 Rheology of micellar solutions

In order to interpret the rise of bubbles in micellar solutions, we need to determine the viscoelastic properties of the solutions, which depend on the concentration of NaSal. The increase in the concentration of NaSal causes the micelles to gradually change from small elliptical ones to long tangled wormlike micelles, and the solutions become viscoelastic [10].

We have measured the flow curves of mixed solutions for 20 mM CTAB and different NaSal concentrations, as shown in Figure 1. These solutions exhibit two types of behaviour. At low shear rates, $\dot{\gamma}$, viscosity is independent of shear rate, however above a critical shear rate they become shear thickening (empty symbols) or shear thinning (filled symbols).

For pure CTAB solution and CTAB solutions with low NaSal concentrations (0, 2, 4, 8, 9 mM empty symbols), at low shear rates, the viscosity is independent of shear rate, and they behave as Newtonian fluids. As the concentration of NaSal increases to 8 and 9 mM, the viscosity of the solution increases to several times that of pure CTAB solution. At high shear rates (30-100 $s^{-1}$), a shear thickening behaviour is observed. As will be seen later, the shear rates experienced by the bubbles are smaller so we will call these solutions "Newtonian" in the following.

In the solutions at higher concentrations (NaSal concentration = 10, 11, 11.5, 12, 12.5, 13 mM, filled symbols) a viscosity plateau (zero-shear-rate viscosity) at low shear rates is observed, which is followed by a shear thinning behaviour. Shear thinning starts at lower shear rates as the concentration of NaSal increases. These samples will be referred to as "shear thinning" in the following.

The response of the solutions to shear can be explained by the structure of the micelles. In pure CTAB solution and at low NaSal concentrations, the surfactants self-assemble into small cylindrical micelles [10,11]. As the concentration of NaSal increases to 8 and 9 mM, the viscosity of the solution increases owing to the growing length of the micelles. This is because more $Sal^-$ ions incorporate into the surfactant layer reducing the electrostatic repulsion between the surfactant head groups. The observed shear-thickening phenomenon is induced by the formation of shear-induced structures, the origin of which is not yet fully understood [12].

When the concentration of NaSal reaches 10 mM, the length of the wormlike micelles is larger and they begin to entangle. As the shear rate increases above a critical value, the solutions

become shear thinning and the viscosity starts to decay as $\dot{\gamma}^{-1}$. This behaviour has been attributed to shear banding [12,13].

The frequency dependence of the shear moduli *G'* and *G"* are shown in Figure SI2. The storage modulus *G'* remains smaller than the loss modulus *G"* up to 10 mM NaSal, meaning that the solutions are predominantly viscous. At larger salt concentration, *G'* become slightly larger than *G"* above frequencies of the order of 1 Hz. Even for the largest salt concentration, the storage modulus is very small (*G'* less than about 1 Pa).

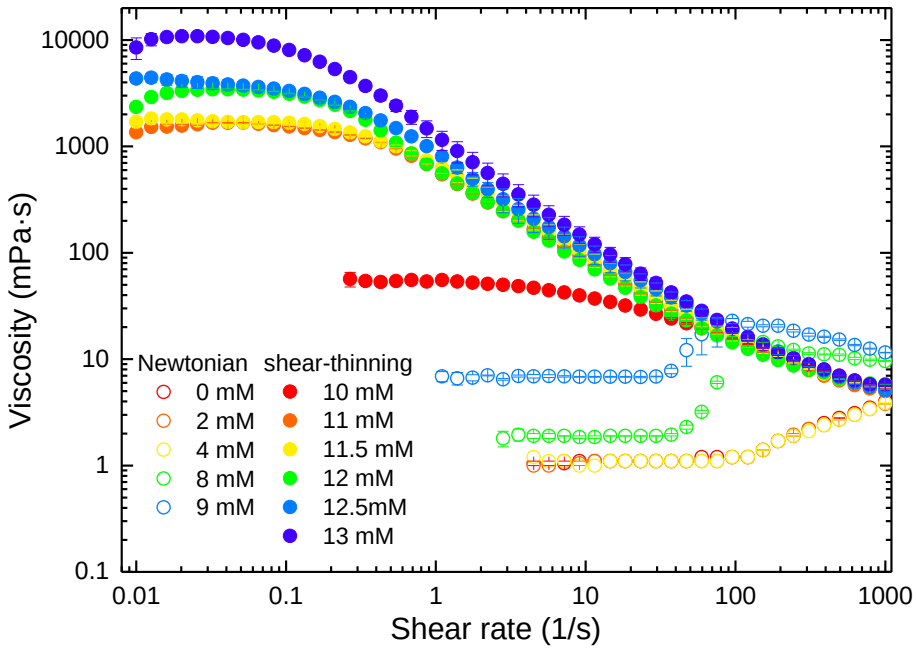


Figure 1. Flow curves of solutions containing CTAB (20 mM) and NaSal (0-13 mM) at 22 °C. The Newtonian solutions have empty symbols and the shear thinning solutions have filled symbols, the NaSal concentrations are indicated in the legend.

### 3.2 Bubble size

Generation of bubbles in viscous fluids is not easy. We made the bubbles using the double syringe method with bubble volume fractions ranging from 5 to 30 %. In this gas fraction range, all the gas is incorporated into the solution. Higher gas volume fractions were not used as all the gas can no longer be incorporated into the most viscous samples. Once the bubbles are formed, their sizes are measured using a Mastersizer 3000. The Sauter radius $R_{32}$ is shown in Figure 2 for all the studied samples. The error bars denote the standard deviation between ten

subsequent measurements. The bubbles made in the Newtonian solutions are shown with empty symbols and the bubbles made in the shear thinning solutions are shown with filled symbols.

Bubble size is smallest for samples with the lowest concentrations of NaSal (0, 2, 4 mM) and remains almost constant until 8 and 9 mM NaSal where a transition to larger bubbles is observed. These two samples are still Newtonian fluids but have higher viscosities than the other samples. For small NaSal concentrations, the average bubble radii are between 12 and 22 μm (still larger with 8 and 9 mM NaSal). The bubble size increases weakly, but systematically, with gas volume fraction $\varphi_{gas}$. The bubble size distributions are shown in Figure SI3. As $\varphi_{gas}$ increases, the bubble size distributions become wider. In the shear thinning solutions, the bubble sizes are larger (between 25 to 35 μm). There is no dependence of the bubble size on the gas fraction, but as with the Newtonian solutions, the bubble sizes have wider distributions at higher gas fractions.

Bubble size is in principle affected by surface tension: the lower the tension, the easier it should be to make bubbles and hence the smaller the radius. Table 1 shows that surface tension decreases with NaSal concentration. This should lead to a smaller bubble size, but this is not what we observe. This suggests that other factors control bubble size. The charge of the bubbles can change as the ionic strength of the samples changes, but as we see no strong effect from 0 to 8 mM NaSal its effect should be weak. In the two syringe method Gaillard *et al*. found that bubble size increases with $\varphi_{gas}$ and decreases with viscosity [9]. The trend observed with $\varphi_{gas}$ with the Newtonian solutions in Figure 2 is consistent with this work, but here the more viscous samples have larger bubbles. In the work of Gaillard *et al.* the solutions used were Newtonian, whereas our solutions are shear-thinning or shear-thickening at high shear rates. In the two-syringe method, as the bubbly liquid passes through the constriction, it experiences high shear rates. We estimated the shear rate from the piston velocity ≈ 10 cm/s and the constriction radius of 2 mm as around 50 $s^{-1}$. This is close to the shear-thinning transition, which makes it hard to predict the viscosity. In any case, a full understanding of the bubble generation in shear thinning viscoelastic fluids is beyond the scope of this paper.

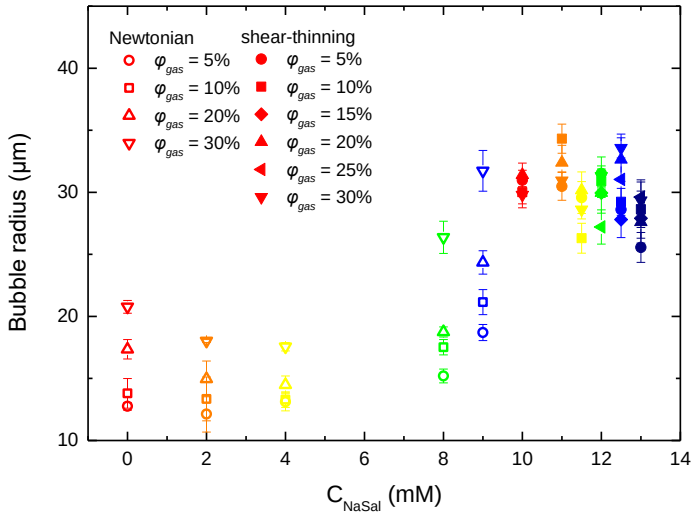


Figure 2. Sauter radius of bubbles produced in solutions with CTAB (20 mM) and NaSal (0-13mM) at 22 °C. The corresponding bubble size distributions can be found in the supporting information Figure SI3.

### 3.3. Measure of the bubble rise velocity

In order to investigate how bubbles rise in the CTAB/NaSal solutions, we took photographs of bottles filled with bubbly liquids in transmission to track the rise of the bubble front. Figure 3 (a) shows photographs of the bottles during bubble rise in solutions containing 20 mM CTAB/4 mM NaSal and $\varphi_{gas}$ = 5%. The bubbly liquid appears black, as the bubbles scatter light strongly. In time, bubbles rise and a front between the bubbly liquid and the clear liquid (devoid of bubbles) becomes visible. The front moves upwards in time and we measure the bubble rise velocity from the evolution of its position using the Image J software.

The grey values in our images vary between 0 and 160. We chose three grey values $I$ = 40, 80 and 120 (smaller $I$ means darker regions) and measured the corresponding front position height versus time. The results are shown in Figure 3b. The front position varies linearly with time, but the rise velocities for each grey value are different: 0.32 mm/s for $I$ = 40, 0.25 mm/s for $I$ = 80, 0.21mm/s for $I$ = 120. The differences are due to the finite width of the front caused by the polydispersity in bubble size. As the smallest bubbles rise more slowly, the largest $I$ will be sensitive to the smallest bubbles.

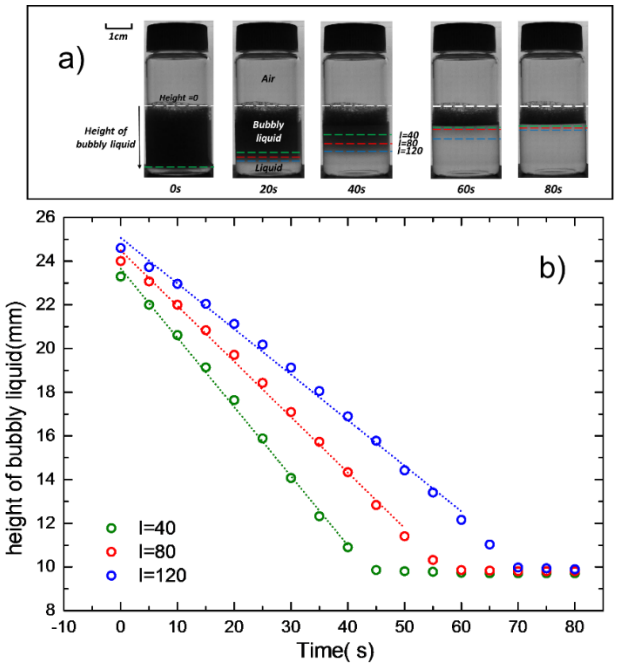


Figure 3. (a) Images of the bottles containing bubbly liquids at different times, showing the front evolution. The three horizontal lines (green, red and blue) indicate the position of the front for the three different grey levels $I$ = 40, 80 and 120, respectively. (b) Height of bubbly liquid versus time for different grey levels. Solution with 20 mM CTAB and 4 mM NaSal and $\varphi_{gas}$= 5%

The front velocities are constant in time for all samples (different NaSal concentrations and gas fractions), except for the largest NaSal concentration (13 mM). In this sample, and for all bubble volume fractions, the velocity changes with time, as shown in the example of $\varphi_{gas}$= 5% in Figure 4. In Figure 4a, photographs of the bottles at different stages of the bubble rise process are shown, while the variations of front positions height with time (for $I$ = 40, 80 and 120) are shown in Figure 4b. We can observe an initial "fast" rise of the bubbles during a few 100 seconds (as seen in the inset of Figure 4b). After this, the bubbles slow down dramatically and the rise process takes more than 15 hours. The final photograph of Figure 4a is taken after 63 000 s (17.5 hours) after the start, and some small bubbles still remain suspended in solution. Before comparing the bubble rise velocities to the predictions, the expected bubble rise regimes will be discussed.

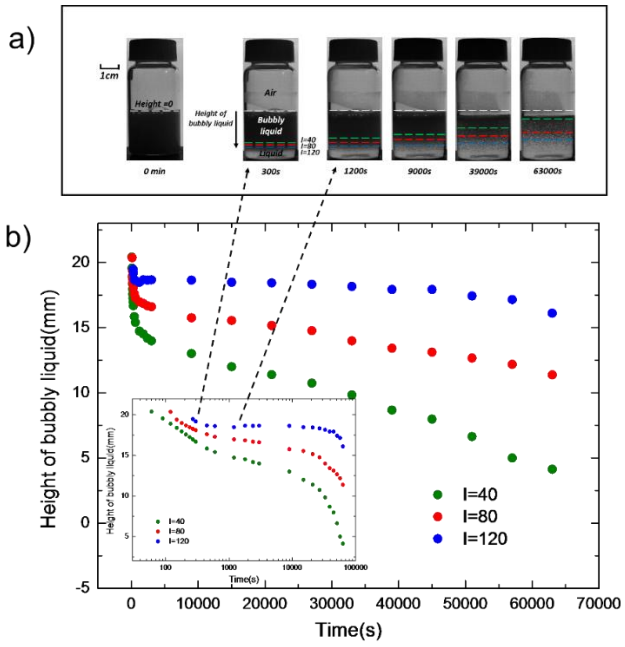


Figure 4. (a) Images of the bottles containing bubbly liquids at different times, showing the front evolution at the different intensity levels $I$ = 40 (green), 80 (red) and 120 (blue). The white line indicates the level of the bubbly liquid at the beginning of the experiment. (b) Height of bubbly liquid versus time for different grey levels. The inset is a semi-logarithmic plot. The system shown in the image is a solution with 20mM CTAB and 13 mM NaSal at $\varphi_{gas}$= 5%.

### 3.4. Bubble rise regime

Bubble rise is known to depend on several factors: Reynolds number; bubble surface boundary condition and; whether the bubbles can deform or not. We studied relatively small bubbles ($R < 35$µm), for which the Reynolds number $Re$ is small

$$Re = \frac{2\rho v R}{\eta} \tag{1}$$

where $\rho$ and $\eta$ are respectively the fluid density and viscosity, $v$ the velocity, and $R$ the bubble radius. For pure CTAB solutions, using $\rho$ = $10^3$ kg/m$^3$, $\eta$ = 1 mPa/s, $v$ = 0.3 mm/s, $R$ = 20 µm, we find $Re \sim 10^{-2}$. For the shear thinning solutions, $v$ decreases and $\eta$ increases so $Re$ decreases. Therefore, the experiments were all carried out in a region of small $Re$.

Bubbles remain spherical if both the inertial and viscous forces are small compared to surface tension forces [14]. This happens when the Weber number $We$ and the capillary number $Ca$ are small:

$$We = \frac{\rho v^2 R}{\gamma} \qquad Ca = \frac{\eta v}{\gamma} \tag{2}$$

Here, with γ = 35 mN/m, $We \sim 10^{-7}$ and $Ca \sim 10^{-5}$ are both very small for pure CTAB solutions. For the solutions with NaSal, the viscosity increases but the velocity decreases, so both numbers remain small, and we can safely assume that our bubbles are not deformed during the rise process.

A further question concerns the boundary condition at the bubble surface, which would change the bubble rise velocity. In dilute surfactant solutions and for small Reynolds numbers, the surfaces of rising bubbles are immobilised by surface tension gradients and Marangoni forces created by the liquid flow: surfactant is depleted from the bubbles' apex and it accumulates at their rear. The bubbles behave as solid particles [2]. When surfactant concentration is higher, the depleted surfaces can be replenished by surfactant adsorbing from the bulk. The problem was discussed in detail by Maldarelli and co-workers [14] who predicted that the Marangoni force is larger for smaller bubbles. Above the critical micellar concentration, the adsorption kinetics is also controlled by the micelle lifetime, which is very long (minutes) in the presence of salt. It is therefore likely that in our experiments, the bubble surfaces can be considered as immobile.

In this case the bubble rise velocity for a single bubble in a Newtonian fluid would be given by the Stokes expression:

$$v_s = \frac{2\rho g R^2}{9\eta} \tag{3}$$

The Stokes expression is valid for a single particle and corrections have been proposed to account for the influence of particle concentration. Corrections to the rise (or sedimentation) velocity are required to take into account additional hindering effects, both from the proximity of neighbouring particles, and the flow of liquid as it is displaced by the rising (descending) particles. When the particles behave as hard spheres, the phenomenological expression of Richardson-Zaki [15] is accurate up to large volume fractions:

$$v = v_s(1-\varphi)^n \tag{4}$$

Here $\varphi$ is the particle volume fraction. The exponent $n$ varies with the Reynolds number $Re$ and has been shown to vary from 4.8 in the viscous regime down to 2.4 in the inertial regime [16]. In our experiments, $Re \approx 10^{-2}$ we can expect it to be close to 4.8. We use $n = 4.5$ close to

values used in the limit of small *Re* in simulations of bubble rise [17] and studies of sedimentation of solid particles [18,19].

### 3.5. Bubble rise in Newtonian solutions

In the following we use the bubble rise velocities measurements with $I$ = 80, which is the average grey value in the rising front. Results for other $I$ values could be found in the SI (Figures SI6 and SI7).

Figure 5 shows the variation of the bubble rise velocity normalised by Stokes velocity ( $v/v_s$) as a function of gas fraction ($\varphi_{gas}$) for the Newtonian solutions measured with $I$ = 80. The different velocities collapse onto a single master curve, as expected for Newtonian fluids. We calculated $v_s$ using equation 3 with the experimentally measured viscosities and Sauter radii. We used the radii measured just after generation, as we do not expect the bubble size to change during their rise. This is because Ostwald ripening is too slow to change it during the rise process and we do not observe any coalescence. We can estimate the rate of Ostwald ripening which does not change much with bubble volume fraction [20] and is given for small $\varphi_{gas}$ by

$$\Omega = \frac{dR^3}{dt} = \frac{8}{9} \frac{\gamma D_m He*}{P} \quad (5)$$

where $D_m$ is the gas diffusion coefficient in water, $He*$ is the Henry constant expressed as the volume fraction of gas in water and $P$ is the atmospheric pressure. For bubbles with $R$ = 20 μm in water, $D_m = 2.6 \times 10^{-9}$ m$^2$/s and $He* = 0.013$, which results in $\Omega \sim 10^{-17}$ m$^3$/s, and an increase in radius of about 2 μm in 100 s.

We cannot follow individual bubbles as they rise to see if they coalesce or not. However, once all the bubbles have reached the top of the solution and formed a froth, its height remains constant, confirming the absence of coalescence. The concentration of bubbles in the froth at the top is much higher than while they are rising. In general, a higher volume fraction leads to more coalescence, therefore we do not expect any significant coalescence during the bubble rise process either.

Small bubbles rise sufficiently slowly and the shear rate is small enough, so that the solution viscosity remains Newtonian throughout the process. For the least viscous sample with 20 mM CTAB/4 mM NaSal at $\varphi_{gas}$ = 5 % the velocity is the highest (0.25 mm/s). At this velocity, we have the maximum shear on the bubbles, which we can estimate as $\dot{\gamma} = v/R \sim 20$ s$^{-1}$. This shear rate is lower than the shear rate at the onset of shear-thickening and the liquids remain Newtonian during the front motion.

The Richardson-Zaki prediction calculated using Equation 4 is shown in Figure 5 with a black dashed line. We can see that within error bars, the data is in good agreement with the model. In the limit of $\varphi_{gas} = 0$ the rise velocity coincides with the Stokes velocity, the velocity of a single bubble rising in an infinite medium, calculated with the average Sauter radius, confirming that the bubbles behave as solid particles, as the velocity would have been higher if the bubble surfaces were mobile. In Figure SI6 and Figure SI7, the data for $I$ = 40 and $I$ = 120 are also shown. The former is slightly above the R-Z curve, while the latter is below the Richardson-Zaki curve. This is because the bubbly liquids are polydisperse, and at $I$ = 40 we follow the largest bubbles, while at $I$ = 120, we follow the smallest ones.

Literature on the velocity of the sedimentation or rise front in solid particles or oil drops is abundant [21]. However, measures of the bubble rise front and comparison with Richardson-Zaki are scarce although it has been used in gas flotation modelling [22]. We show that in the limit of small bubbles in high concentrations of surfactant, the rise velocity is well captured by Richardson-Zaki, which does not work when larger bubbles are used [23].

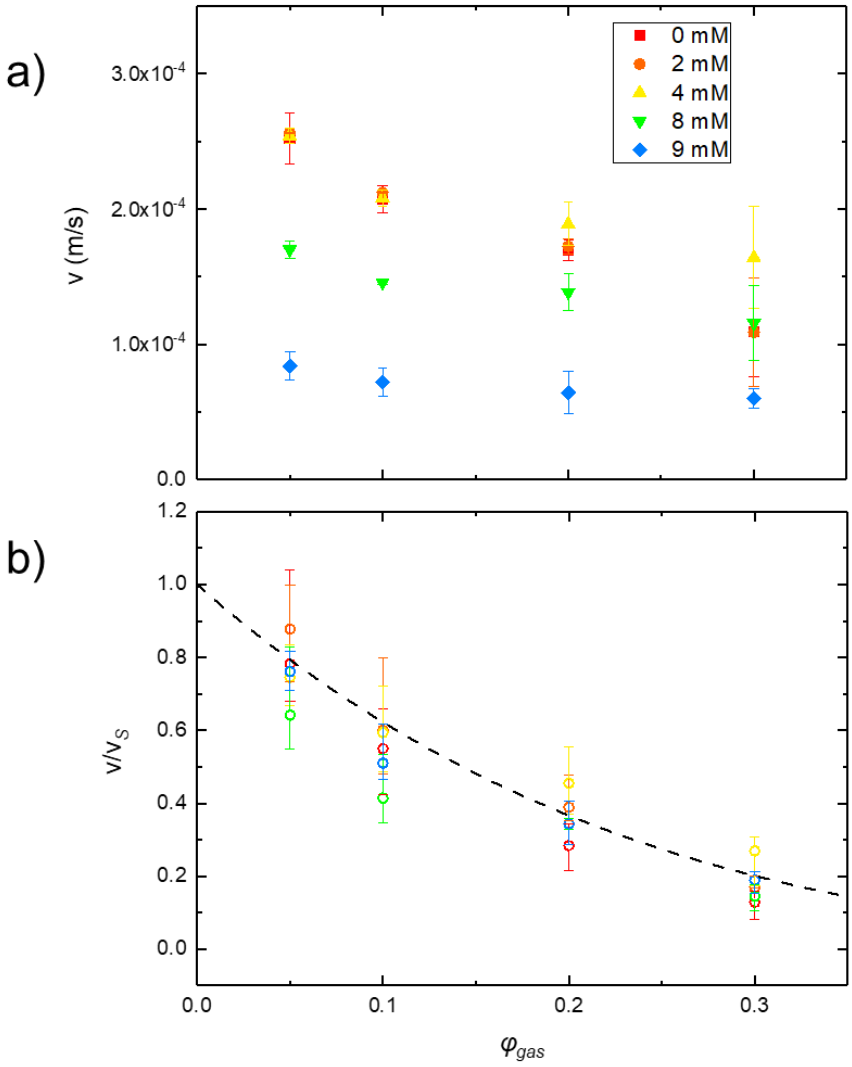


Figure 5. a) Bubble rise velocity $v$ as a function of gas volume fraction for the Newtonian solutions. b) $v$ normalised using the Stokes velocity $v_s$, as a function of gas fraction. The dashed line is the Richardson-Zaki prediction of equation (4) with $n$ = 4.5 The velocities are measured from $I$ = 80.

### 3.6 Bubble rise velocity in shear thinning solutions

For the shear thinning solutions, the initial front velocities are shown in Figure 6a as a function of gas volume fraction. As in the Newtonian solutions, the velocity decreases with increasing NaSal concentration, so with increasing viscosity of the samples. In order to better compare the allure of the $\varphi_{gas}$ dependencies, we normalised the velocities with the velocity at $\varphi_{gas}$ = 0.05. The results are shown in Figure 6b, with the predicted evolution by Richardson-Zaki shown as the black dashed line. The decrease of the rise velocity with gas fraction is much

weaker than predicted by Equation 4 and almost vanishes at large NaSal concentration. Therefore, the Richardson-Zaki prediction does not apply here. The weak variation of the velocity as a function of $\varphi_{gas}$ can be described using

$$\frac{v}{v(\varphi_{gas}=0.05)} = 1.1\left(1 - \varphi_{gas}\right) \tag{6}$$

which has been shown in Figure 6(b) the purple dotted line. Gummalam and Chhabra predicted bubble rise velocities at different gas volume fractions in shear thinning fluids [24]. They saw a weaker decrease of the rise velocity with $\varphi_{gas}$ compared to Newtonian fluids and Richarson Zaki. This was attributed to an increased shear at higher $\varphi_{gas}$, which leads to a decreased viscosity. If the decrease in viscosity was sufficiently important (in strongly shear thinning fluids) a maximum in the rise velocity at an intermediate $\varphi_{gas}$ was predicted. We see something close to this in the most viscous samples where the bubble rise velocity can be higher at higher $\varphi_{gas}$ as seen with the samples with 12.5 and 13 mM of NaSal.

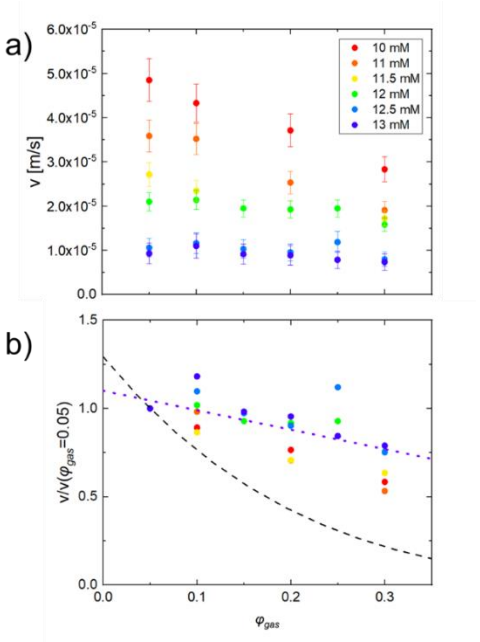


Figure 6. (a) Front rise velocity, $v$ as a function of $\varphi_{gas}$ for the shear thinning solutions, i.e., CTAB 20 mM with NaSal 10-13 mM indicated in the legend. The velocities are measured using $I$ = 80. (b) Front velocity normalised by the velocity at $\varphi_{gas}$= 0.05, the dashed line shows the prediction of Richardson-Zaki equation. The weak variation of the velocity as a function of $\varphi_{gas}$ can be described using Equation 6(the dotted purple line).

Evolution of bubble rise velocity with $\varphi$ in shear thinning fluids is different than in Newtonian solutions, however this might be because the viscosity experienced by the bubbles

depends on their rise velocity. The bubble rise velocities can be compared to those found in Newtonian solutions if we can estimate the viscosity experienced by the bubbles as they rise (as done for the sedimentation of a single particle in viscoelastic solutions by Gheissary et al for example [25]). For each concentration, we used the velocity at $\varphi_{gas}$ = 0.05 and an average bubble radius $\langle R \rangle$ of 30 μm to estimate the shear rate in the sample as

$$\dot{\gamma} = \frac{v\,(\varphi_{gas}=0.05)}{R} \tag{7}$$

$v_s(\eta)$ is calculated for each sample using equation 3 with $\eta(\dot{\gamma})$ and $R$. The front velocities normalised by $v_s(\eta)$ are shown in Figure 7.

For the sample at NaSal = 10 mM (red points) the normalised velocities with the estimated $v_s(\eta)$ are close to 1 (between 0.7 and 1.2). This can be explained by the low shear rate experienced by the bubbles at 1.6 $s^{-1}$, which lies on the Newtonian plateau. However, for all of the other samples, the situation is very different, and the measured velocities are around 10 times higher than the Stokes velocity (for NaSal = 13 mM they are almost 20 times higher). Either our estimation of the shear rate and hence the viscosity is poor, or the bubbles are in a different bubble rise regime.

The viscosity depends on our estimation of the shear rate, and instead of using the bubble radius to define the length-scale we could have used the average inter-bubble distance. However, this distance is higher than the radius (with $R$ = 30 μm) for all the gas volume fractions, so its use would lead to a lower predicted shear rate and a higher viscosity. Hence, its use could only increase the disagreement between the Stokes prediction and the measured velocity. Therefore, we are missing something in our description of the bubble rise. Possibly the distance between the bubbles is smaller due to clustering, as this would lead to higher shear rates and lower viscosities.

Indeed, Vélez-Cordero and Zenit showed that at small *Re* and large *Bo*, bubbles cluster while they rise [26]. The clustering could be predicted from studies on pairs of bubbles and it is due to attractive hydrodynamic interactions acting via the bubbles' wake. The studies were done with much lower $\varphi_{gas}$ and larger monodisperse bubbles. Comparing to their predictions, the bubbles in our systems could be expected to be in the clustering regime. We show photographs of a close up of bubbles rising in a Newtonian fluid at $\varphi_{gas}$ = 0.01 (4 mM NaSal in Figure 7b) and in a shear thinning fluid at $\varphi_{gas}$ = 0.01 (12 mM NaSal in Figure 7c). The difference between the two images is striking. In the Newtonian solution the bubbles remain homogeneously distributed in the fluid during the rise process, however in the shear thinning sample a heterogeneous distribution of bubbles is evident. The distance between the bubbles decreases, as the effect of shear thinning dominates over the hindering due to the proximity of the

neighbours. The structuration within the sample, or clustering could explain the faster than expected bubble rise velocity of Figure 7.

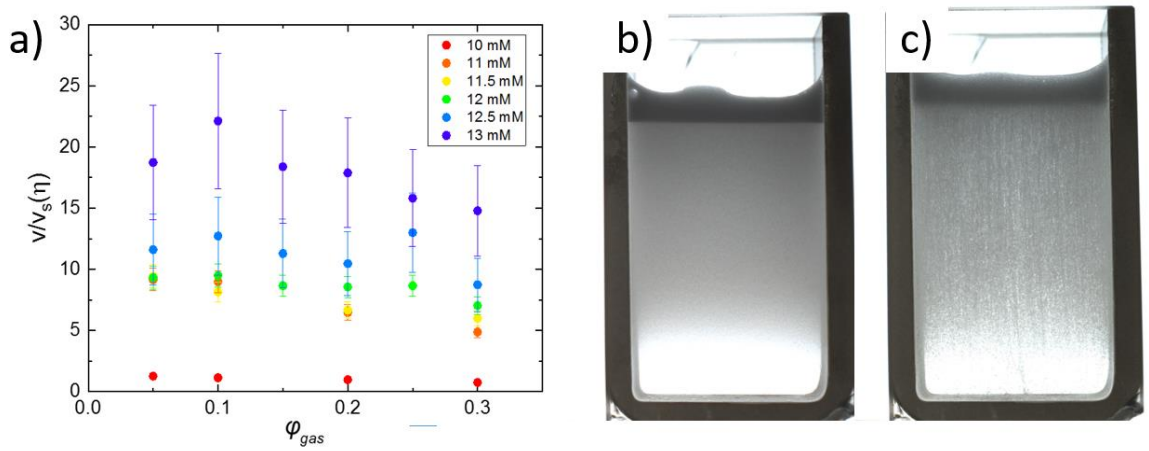


Figure 7. a) Bubble front rise velocity $v$ of the shear thinning samples normalised by the Stokes velocity calculated using $\eta$ estimated at the shear rate around the bubbles $v/R$ (as explained in the text). Photographs of bubbles rising in a sample with CTAB 20 mM and NaSal 4 mM where the bubble dispersion remains homogeneous b) and in a sample with CTAB 20 mM and NaSal 4 mM where the bubble dispersion is develops an inhomogeneous distribution, seen as the streaks c).

Another peculiarity of bubbles' motion observed for the most viscous liquid (13 mM NaSal) is the fact that it slows down considerably after some tens of minutes, as seen in Figure 4. The second bubble rise velocity is also quite constant in time; it is shown with the initial velocity in Figure 8. The second velocity is around $10^{-7}$ m/s, which is 100 times slower than the initial velocity.

If we look at the photographs in Figure 4a corresponding to the slow rise regime, we can see that the volume fraction of bubbles left is relatively small, with most of the bubbles having risen during the first stage. The samples are polydisperse and the smallest bubbles lag behind. If we use the bubble rise velocity to again estimate the shear rate, we find $\dot{\gamma} \approx 10^{-2}$ s$^{-1}$, which is on the Newtonian plateau with $\eta\,(\dot{\gamma} = 10^{-2}\ \mathrm{s}^{-1}) = 10^{7}$ Pa.s. We have seen that on the Newtonian plateau, the Stokes velocity compares well with the rise velocity; therefore, we can estimate the size of bubbles rising at such slow velocities. We find $R$= 22 µm, which is in the tail of the bubble size distribution (around 10% of the bubbles). This suggests that how the bubbles rise could be different depending on their size within the polydisperse samples. The larger bubbles rise fast enough to experience shear rates within the shear-thinning regime, while the smaller

bubbles rise so slowly that they experience shear rates on the Newtonian plateau and hence maximum fluid viscosity. It might also be that the smaller bubbles cluster less than the larger ones, which would lead to a significant decrease in the rise velocity.

We do not see such a slow rising population of bubbles at the lower concentrations of NaSal. This is because even for the next sample with 12.5 mM NaSal, the plateau viscosity is 3.9 Pa.s, which means that only bubbles with $R < 13$ µm would reach the second creaming regime of constant velocity. The tail of the bubble size distribution for 13 mM NaSal is very close to this value and there are hardly any bubbles of this size in the other samples. This could explain why we do not observe the slower bubble rise in the other samples.

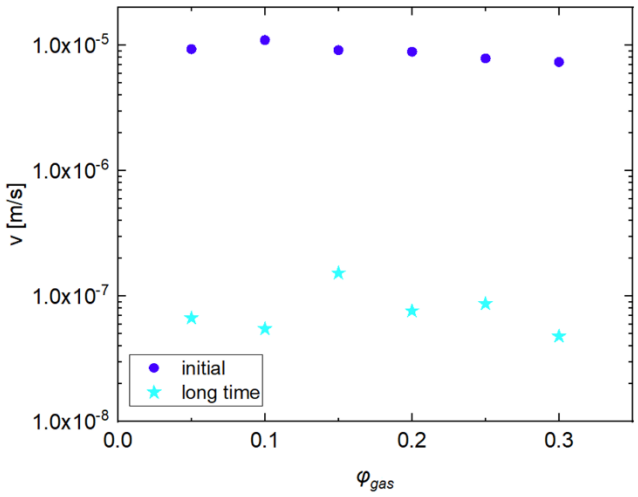


Figure 8. The front rise velocity $v$ of the initial bubble rise, and the velocity at long times, once it has considerably slowed down. Both were measured using $I$ = 80. Solution with 20mM CTAB and 13 mM NaSal at $\varphi_{gas}$= 5%.

### 3.7 Flotation in a shear thinning fluid

Foam flotation is used to purify and separate materials from fluids: the material attaches onto the bubble surfaces, which rise up for separation. An important parameter to quantify foam flotation is the bubble surface area flux $\dot{S}$, which tells how much surface area is swept up per second and is directly linked to how efficiently the process works [27,28]. In a bubble column, $\dot{S}$ is given by the product of the average bubble rise velocity $v(\varphi_{gas})$ and the number density of bubbles $N \propto \frac{\varphi_{gas}}{R}$ as $\dot{S} = v(\varphi_{gas})\frac{\varphi_{gas}}{R}$. As $v$ varies very differently in the Newtonian and the shear thinning fluids, we can expect $\dot{S}$ to change.

In Newtonian fluids, the Richardson-Zaki expression works well, which is $v_{Newt} \propto (1-\varphi_{gas})^{4.5}$ as given by equation 4. For the shear thinning fluids, velocity depends more weakly on $\varphi_{gas}$ as given by equation 6. Variation of the velocity can be reasonably described by $v_{Non-Newt} \propto (1-\varphi_{gas})^{1}$, as shown by the purple dotted line in Figure 6b. We can therefore use the two expressions for velocity to estimate $\dot{S}$ in Newtonian and shear thinning fluids, as has been done before for Newtonian fluids [22]. This results in very distinctive bubble surface area variations with $\varphi_{gas}$, as shown in Figure 9. Indeed, if maximisation of the bubble surface area flux is an objective, in Newtonian fluids the optimum is at $\varphi_{gas}$ = 0.16, while in shear thinning fluids, higher $\varphi_{gas}$ would improve the area flux. Our experiments are limited to gas fractions less than 0.3, and we cannot speculate about what happens at higher $\varphi_{gas}$. However, our results suggest that the parameters for optimum flotation where shear thinning viscoelastic fluids are present can be very different from those with Newtonian fluids.

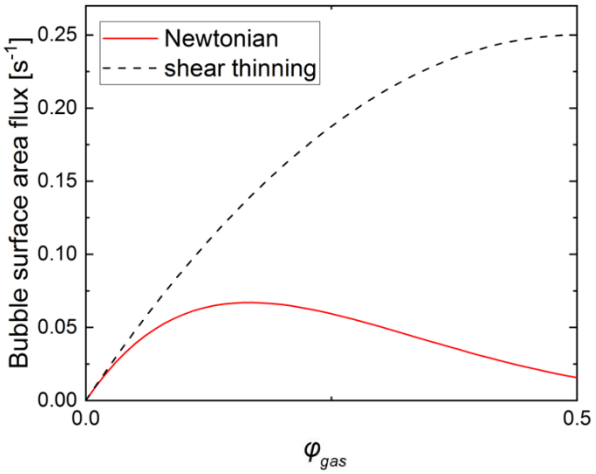


Figure 9. Bubble surface area flux as a function of bubble volume fraction for Newtonian and shear thinning viscoelastic fluids. The dependence is very different, and the maximum in shear thinning fluids occurs at a much higher $\varphi_{gas}$.

## 4. Conclusion

We show that it is possible to generate bubbly suspensions up to gas fractions of 30 % with bubble radii between 15 - 35 µm in radius using the two-syringe method from shear thinning viscoelastic fluids. We measured the rise velocity of the bubbles in viscoelastic fluids of varying viscosity and shear dependence. We show that in Newtonian fluids bubble rise can be described using the Richardson-Zaki law. In shear thinning viscoelastic fluids the bubble rise is much

faster than predicted by the Richardson-Zaki law. The increased shear with the proximity of neighbours leads to a weaker decrease of the rise velocity with phi as it partly compensates for the hindering due to the increased proximity of neighbours. The distribution of bubbles becomes heterogeneous and the bubble clustering is observed. In the most viscous sample, we measured two distinct velocities for the bubble rise front.

Previous work on generating foams in viscous Newtonian fluids showed a decrease of bubble size with viscosity [9]. However, we see the inverse effect in the viscoelastic shear thinning fluid, the origin of which remains to be explored.

The very small bubbles studied prevented the hydrodynamic instabilities observed in gravity driven bubbly flows with millimetric bubbles. They rise more slowly, and the Reynolds numbers are small. This allowed us to observe the formation of a front between the pure liquid and liquid containing close packed bubbles, a feature observed with emulsions where sedimentation or creaming fronts are commonly reported in the literature [21]. However, measures of such fronts in bubbly flows are scarce. That the Richardson-Zaki law works well with the small bubbles confirms that the surfaces are immobilised, in agreement with the predictions of Maldarelli et al who showed that surface tension gradients are more effective in immobilising surfactant layers in small bubbles than in large ones [29].

Bubbles in the non-Newtonian solutions studied rise much more rapidly than expected considering the viscosity of the solutions. We propose that this is due to bubble clustering, a phenomenon that had been observed in such fluids, but only up to 1 % of gas fraction [1]. We show that the bubble rise velocity is strongly enhanced up to gas fractions of 30 %. These observations require further experimental and theoretical studies to understand the exact interactions between bubbles.

From a practical point of view these results could have important implications to flotation in viscoelastic fluids. The area flux has a very different dependency on gas volume fraction in viscoelastic shear thinning fluids compared to Newtonian ones (calculated previously [22]), and thus it impacts directly on flotation performance. These predictions should be tested in dedicated flotation settings.

**Acknowledgements**

Q.C. thanks Prof. Yazhuo Shang and the China Scholarship Council for one and a half year exchange fellowship during his thesis.

References


[1] Zenit R, Feng JJ. Hydrodynamic Interactions Among Bubbles , Drops , and Particles in Non-Newtonian Liquids. Annu Rev Fluid Mech 2018;50:505–34.

[2] Clift R, Grace JR, Weber ME. Bubbles, drops, and particles. Courier Corporation; 2005.

[3] Levich VG. Physicochemical hydrodynamics. Englewood Cliffs, N.J.: Prentice-Hall; 1962.

[4] Kulkarni AA, Joshi JB. Bubble Formation and Bubble Rise Velocity in Gas-Liquid Systems : A Review 2005:5873–931.

[5] Dollet B, Marmottant P, Garbin V. Bubble dynamics in soft and biological matter. Annu Rev Fluid Mech 2019;51:331–55. https://doi.org/10.1146/annurev-fluid-010518-040352.

[6] Jakobsen HA, Sannæs BH, Grevskott S, Svendsen HF. Modeling of Vertical Bubble-Driven Flows. Ind Eng Chem Res 1997;36:4052–74. https://doi.org/10.1021/ie970276o.

[7] Rothstein JP, Mohammadigoushki H. Journal of Non-Newtonian Fluid Mechanics Complex flows of viscoelastic wormlike micelle solutions 2020;285.

[8] Kostrzewa M, Delgado A, Wierschem A. Particle settling in micellar solutions of varying concentration and salt content. Acta Mech 2016;227:677–92. https://doi.org/10.1007/s00707-015-1472-6.

[9] Gaillard T, Roché M, Honorez C, Jumeau M, Balan A, Jedrzejczyk C, et al. Controlled foam generation using cyclic diphasic flows through a constriction. Int J Multiph Flow 2017;96:173–87. https://doi.org/10.1016/j.ijmultiphaseflow.2017.02.009.

[10] Lam CN, Do C, Wang Y, Huang GR, Chen WR. Structural properties of the evolution of CTAB/NaSal micelles investigated by SANS and rheometry. Phys Chem Chem Phys 2019;21:18346–51. https://doi.org/10.1039/c9cp02868d.

[11] Clausen TM, Vinson PK, Minter JR, Davis HT, Talmon Y, Miller WG. Viscoelastic micellar solutions: Microscopy and rheology. J Phys Chem 1992;96:474–84. https://doi.org/10.1021/j100180a086.

[12] Cates ME, Fielding SM. Rheology of giant micelles. Adv Phys 2006;55:799–879. https://doi.org/10.1080/00018730601082029.

[13] Padding JT, Briels WJ, Stukan MR, Boek ES. Review of multi-scale particulate simulation of the rheology of wormlike micellar fluids. Soft Matter 2009;5:4367–75. https://doi.org/10.1039/b911329k.

[14] Palaparthi R, Papageorgiou DT, Maldarelli C. Theory and experiments on the stagnant cap regime in the motion of spherical surfactant-laden bubbles. J Fluid Mech 2006;559:1. https://doi.org/10.1017/S0022112005007019.

[15] Richardson JF, Zaki WN. The sedimentation of a suspension of uniform spheres under conditions of viscous flow. Chem Eng Sci 1954;3:65–73. https://doi.org/https://doi.org/10.1016/0009-2509(54)85015-9.

[16] Kramer OJI, de Moel PJ, Baars ET, van Vugt WH, Padding JT, van der Hoek JP. Improvement of the Richardson-Zaki liquid-solid fluidisation model on the basis of hydraulics. Powder Technol 2019;343:465–78. https://doi.org/10.1016/j.powtec.2018.11.018.

[17] Sankaranarayanan K, Shan X, Kevrekidis IG, Sundaresan S. Analysis of drag and virtual mass forces in bubbly suspensions using an implicit formulation of the lattice Boltzmann method. J Fluid Mech 2002;452:61–96. https://doi.org/10.1017/S0022112001006619.

[18] Blazejewski R. Apparent viscosity and settling velocity of suspensions of rigid monosized spheres in Stokes flow. Int J Multiph Flow 2012;39:179–85. https://doi.org/10.1016/j.ijmultiphaseflow.2011.10.006.

[19] Nicolai H, Herzhaft B, Hinch EJ, Oger L, Guazzelli E. Particle velocity fluctuations and hydrodynamic self-diffusion of sedimenting non-Brownian spheres. Phys Fluids 1995;7:12–23.

[20] Taylor P. Ostwald ripening in emulsions. Adv Colloid Interface Sci 1998;75:107–63. https://doi.org/10.1016/s0001-8686(98)00035-9.

[21] Aronson MP. The Role of Free Surfactant in Destabilizing Oil-in-Water Emulsions. Langmuir 1989;5:494–501. https://doi.org/10.1021/la00086a036.

[22] Baynham S, Ireland P, Galvin K. Enhancing ion flotation through decoupling the overflow gas and liquid fluxes. Minerals 2020;10:1–17. https://doi.org/10.3390/min10121134.

[23] Loisy A, Naso A, Spelt PDM. Buoyancy-driven bubbly flows: Ordered and free rise at small and intermediate volume fraction. J Fluid Mech 2017;816:94–141. https://doi.org/10.1017/jfm.2017.64.

[24] Gummalam S, Chhabra RP. Rising velocity of a swarm of spherical bubbles in a power law non-newtonian liquid. Can J Chem Eng 1987;65:1004–8. https://doi.org/10.1002/cjce.5450650616.

[25] Gheissary G, Van Den Brule BHAA. Unexpected phenomena observed in particle settling in non-Newtonian media. J Nonnewton Fluid Mech 1996;67:1–18. https://doi.org/10.1016/S0377-0257(96)01436-X.

[26] Vélez-Cordero JR, Sámano D, Yue P, Feng JJ, Zenit R. Hydrodynamic interaction between a pair of bubbles ascending in shear-thinning inelastic fluids. J Nonnewton Fluid Mech 2011;166:118–32. https://doi.org/10.1016/j.jnnfm.2010.11.003.

[27] Prakash R, Majumder SK, Singh A. Flotation technique: Its mechanisms and design parameters. Chem Eng Process - Process Intensif 2018;127:249–70. https://doi.org/10.1016/j.cep.2018.03.029.

[28] Finch JA, Xiao J, Hardie C, Gomez CO. Gas dispersion properties: bubble surface area flux and gas holdup. Miner Eng 2000;13:365–72. https://doi.org/10.1016/S0892-6875(00)00019-4.

[29] Palaparthi R, Papageorgiou DT, Maldarelli C. Theory and experiments on the stagnant cap regime in the motion of spherical surfactant-laden bubbles. J Fluid Mech 2006;559:1–44. https://doi.org/10.1017/s0022112005007019.